ACS OMEGA

http://pubs.acs.org/journal/acsodf

Article

Development of Pipetteless Paper-Based Analytical Devices with a Volume Gauge

Kaewta Danchana,* Hiroshi Iwasaki, Yada Thayawutthikun, Phoonthawee Saetear, and Takashi Kaneta*

Cite This: *ACS Omega* 2023, 8, 11213−11219

Read Online

ACCESS | Metrics & More | Article Recommendations | Supporting Information

ABSTRACT: In this work, we propose a new design for paper-based analytical devices (PADs) that eliminate the need to use a micropipette for sample introduction. With this design, a PAD is equipped with a distance-based detection channel that is connected to a storage channel that indicates the volume of a sample introduced into the PAD. The analyte in the sample solution reacts with a colorimetric reagent deposited into the distance-based detection channel as the sample solution flows into the storage channel where the volume is measured. The ratio of the lengths of the detection channel and that of the storage channel (D/S ratio) are constant for a sample containing a certain concentration, which is independent of the introduced volume. Therefore, the PADs permit volume-independent quantification using a dropper instead of a micropipette because the length of the storage channel plays the role of a volume gauge to estimate the introduced sample volume. In this study, the D/S ratios obtained with a dropper were comparable to those obtained with a micropipette, which confirmed that precise volume control is unnecessary for this PAD system. The proposed PADs were applied to the determinations of iron and bovine serum albumin using bathophenanthroline and tetrabromophenol blue as colorimetric reagents, respectively. The calibration curves showed good linear relationships with coefficients of 0.989 for iron and 0.994 for bovine serum albumin, respectively.

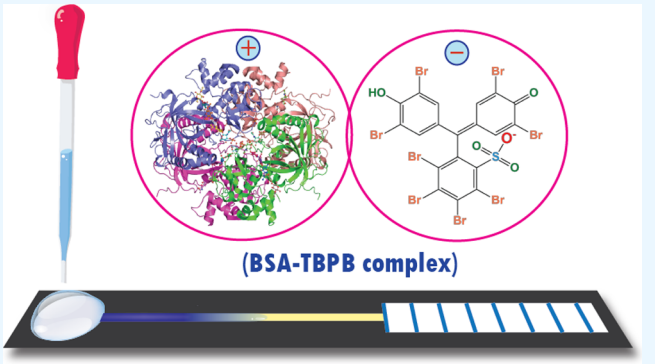

INTRODUCTION

Paper-based analytical devices (PADs) are suitable for point-of-care testing and onsite analysis[1−3] because of their simple manufacture, light weight, affordability, disposability, and transportability.[4] The other advantages of the PADs include simple operations without batteries and/or with only small, portable devices such as smartphones, timers, or miniature detectors. Therefore, outside of equipped laboratories, PADs have become the devices of choice to rapidly determine the concentrations of analytes.

Recently, several studies have demonstrated applications of the PADs to different types of food and environmental samples using detection schemes such as colorimetry,[5−8] electrochemistry,[9−11] fluorometry,[12−14] and chemiluminescence.[15−17] Colorimetry is the most frequently employed detection method because it is simple to achieve qualitative and quantitative analyses of analytes by observing the color change in the detection zones on the PAD. The color images are captured with a digital camera, smartphone, or scanner, which then is followed by image processing using software such as ImageJ.[18,19]

Even though the PADs are a powerful tool for onsite and point-of-care analyses due to their portability and ease of operation to obtain visual results without the need for professional expertise, this technology continues to face numerous obstacles that must be overcome to simplify operations and enhance efficiency. Although spontaneous flow results from the capillary action of the paper fibers in PAD,[20] the flow rate is often too slow to achieve rapid analyses. Researchers have begun to use multilayered paper to accelerate the flow rate.[21] Another shortcoming involves sample introduction that requires the use of an unfamiliar tool for nonexpert technicians in chemical experiments, such as micropipettes to obtain reproducible results.[22] Micropipettes are usually employed for PADs, although many transfer devices are available to allow the subsequent measurement of constant volume: capillary tubes, straws, and loops.[23] Micropipettes typically cost between 25 and 200 USD, depending on the type, and are normally unavailable in less-than-adequately equipped laboratories. These aspects suggest that this process would be more practical without the need for micropipettes. Conversely, several researchers have demonstrated dip-type

Received: December 22, 2022
Accepted: March 6, 2023
Published: March 17, 2023

PADs that permit quantification without the precise introduction of samples.[20,24,25] The dip-type PADs do not require a micropipette because the sample introduction is controlled by the dipping time of the PADs into sample solutions. Therefore, dip-type PADs are more user-friendly than those requiring a micropipette, although precise control of the dipping time is crucial to obtaining reproducible results.

In the present study, we propose a type of PAD that provides reproducible results without using a micropipette for sample introduction—regardless of the sample volume introduced into the device. The PAD consists of an upstream detection channel and a downstream storage channel. The detection channel indicates the sample amount by the length of the colored bar whereas the storage channel plays the role of a volume gauge to estimate the introduced volume. Therefore, the sample is dropped onto the PAD using a plastic dropper or any other common tool, without a specialized tool such as a micropipette to establish a precise volume. Data processing involves measuring the lengths of the detection and storage channels with a ruler to obtain the ratios that are employed for signals to estimate the concentration of the analyte. The calibration curves are constructed by plotting the ratios of the lengths against the concentrations of the analyte. In this way, the proposed PAD is a more user-friendly and facile device than those requiring precise sample introduction. This concept was successfully demonstrated during iron and bovine serum albumin determinations using bathophenanthroline[26] and tetrabromophenol blue,[27] respectively.

EXPERIMENTAL SECTION

Materials. All reagents were of analytical grade and were prepared using deionized water (DI water, resistivity >18 MΩ cm) from an Elix water purification system (Direct-Q UV3, Merck, Darmstadt, Germany). The PADs were fabricated on 200 mm × 200 mm sheets of filter paper (Chromatography Paper 1CHR, Whatman, GE Healthcare Lifescience, UK). Laminate films with a 100 μm thickness consisting of polyethylene terephthalate and ethylene-vinyl acetate were purchased from Monotaro, Hyogo, Japan.

For iron determination, bathophenanthroline (4,7-diphenyl-1,10-phenanthroline), L (+)-ascorbic acid, 2-propanol, and a standard solution of iron (Iron(III) 1000 ppm) were obtained from Fujifilm Wako Pure Chemical Industries, Ltd. (Osaka, Japan). An acetate buffer solution was prepared by mixing acetic acid (Kanto Kagaku Co., Ltd., Tokyo, Japan) and sodium acetate (Nacalai Tesque, Kyoto, Japan). The colorimetric reagent solution contained final concentrations of 1% (w/v) of L (+)-ascorbic acid, 10 mM bathophenanthroline, and 20 mM acetate buffer (pH 4.5) in 80% 2-propanol.

For bovine serum albumin (BSA) determination, citric acid, disodium hydrogen phosphate (Na_2HPO_4), BSA, tetrabromophenol blue (TBPB), and ethanol (EtOH) were purchased from FUJIFILM Wako Pure Chemical Corporation (Osaka, Japan). A citric acid buffer solution was prepared using 0.5 M citric acid and 0.2 M Na_2HPO_4 to adjust the pH to 3. A 1 mM TBPB solution was prepared in a 1:2 (v/v) ratio of ethanol/water.

Design and Fabrication of the PADs. The PADs were designed using PowerPoint 2010 software. A wax printer (ColorQube 8580N, Xerox, CT, USA) printed wax on filter paper to produce the flow channels. The printed sheet was baked at 150 °C for 90 s in an oven (ONW-300S, AS ONE, Tokyo, Japan) to melt the wax ink and penetrate to the backside of the filter paper to create hydrophobic barriers. Two different designs of the PADs were employed for the iron ion and BSA determinations. The designs of the devices are shown in Figure 1. For iron determination, Figure 1A depicts the

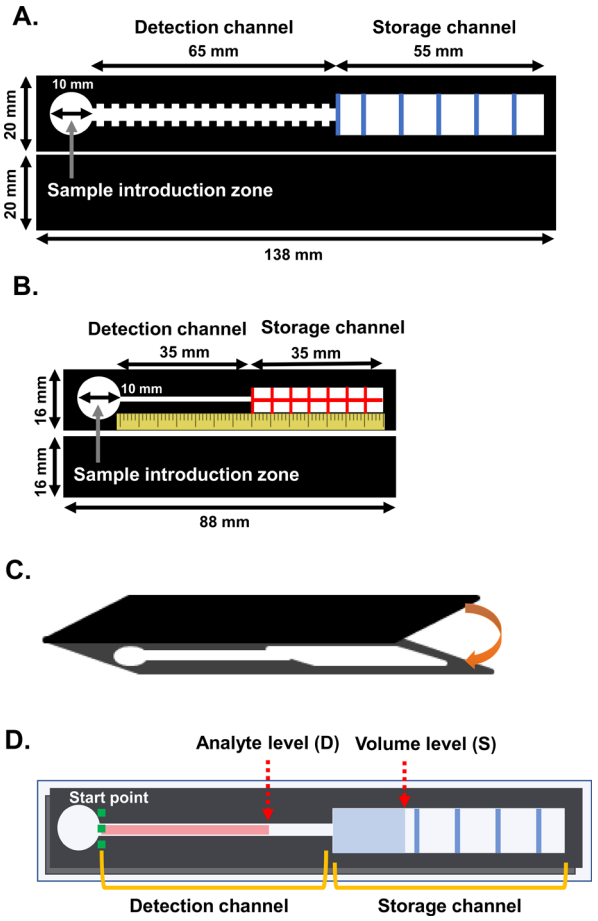

Figure 1. Dimensions of the proposed PADs; (A) PAD for iron determination; (B) PAD for albumin determination; (C) formation of a double layer by folding the PAD; and (D) diagram for data processing.

design using the dimensions of 20 mm in width and 138 mm in length. The detection channel was 65 mm in length and 3 mm in width, and the storage channel was 55 mm in length and 10 mm in width. For BSA determination, the device was designed to be 16 mm in width and 88 mm in length, as shown in the design of Figure 1B where the detection channel was 35 mm in length and 1 mm in width, and the storage channel was 35 mm in length and 6 mm in width. The detection channel for BSA determination had to be smaller than the one for iron determination due to significant dispersion of the colored product in the detection channel.

The PADs for iron determination were prepared by printing the colorimetric reagent solution on the detection channel five times using an inkjet printer (PIXUS, iP2700, Cannon, Tokyo). The ink in the black ink cartridge was removed, followed by washing the cartridge with acetone and water. The cartridge was then filled with the colorimetric reagent solution for printing on the channels of the PADs. Subsequently, blue lines were printed on the storage channel using blue ink in the color ink cartridge of the inkjet printer. The PADs for BSA determination were prepared by dropping the colorimetric

https://doi.org/10.1021/acsomega.2c08138
ACS Omega 2023, 8, 11213−11219

solutions onto the detection channel using a micropipette instead of the inkjet printer because the channel was too narrow to print the reagent solution precisely and accurately. Initially, 5 μL of a citric acid solution was dropped onto the sample introduction zone. Then, a 2 μL aliquot of the citrate buffer solution was dropped onto the detection channel at an interval of 22 mm to occupy the entire detection channel with the citrate buffer solution. After drying the device, a 2 μL aliquot of a TBPB solution was dropped onto the detection channel at an interval of 22 mm as well. After the deposition of the reagent, the color in the detection channel changed from white to light yellow. Subsequently, red lines were drawn in the storage channel using a pen with water-soluble ink. After completing the preparation, the PADs were cut and folded to form double layers, as shown in Figure 1C. Except for the sample introduction zone, the PADs were laminated (KLM42X-W, IRIS OHYAMA, Miyagi, Japan) to prevent the solution from evaporating in the sample solvent (water).

The distance-based readout proved superior to standard colorimetric methods in terms of data processing because it required no device to process the data, whereas a shortage of the analyte solution in a long detection channel could increase analysis time due to a slow flow rate. Layered structures have been used to control the flow rate in the channels of PADs, as described by Channon and co-workers.[28] Therefore, we investigated the effect that a layered structure for the PADs would exert on a distance-based readout.

Samples flow via capillary action and travel in the channel according to the Lucas–Washburn equation shown as eq 1.

$$L(t) = \sqrt{\frac{\gamma r t \cos\theta}{2\mu}} \quad (1)$$

In eq 1, $L(t)$ is the distance of the flowing sample at time, t, γ is the interfacial tension, r is the capillary radius, θ is the fluid contact angle on the paper, and μ is the fluid viscosity. In addition, sample volume, gravity, fiber swelling, and evaporation influence the flow rate in the channel of a PAD. Although these physical parameters are uncontrollable except for the capillary radius when using filter paper, many research groups recently developed PADs that increase the flow rate via hollow channels,[9,29] carved open channels,[30] or multi-layered paper that is either stacked or folded.[31,32] According to Channon et al., a double-layer device showed a more rapid flow rate than those of either single- or triple-layer devices.[28] For iron determination, the single-layer PADs needed 3 h compared with 30 min for a double-layer to flow a sample solution into the storage channel (Figure S1, Supporting Information). For BSA determination, the double-layer structure shortened the time to flow the sample solution of the introduction zone completely from 2 h to 30 min. Thus, the PADs were fabricated with double-layer structures to shorten the analysis time in the present study.

Analytical Procedure. As illustrated in Figure 1, the PAD consists of a sample introduction zone, a detection channel, and a storage channel. When a sample is introduced into the sample introduction zone, the analyte in the sample reacts with the colorimetric reagent in the detection channel. According to the principle of a distance-based PAD, the analytes (ions or molecules) produce a colored bar in the detection channel until all of them complete the reaction with the colorimetric reagent. After consuming all the analytes, only water flows in the channel to reach the storage channel, as illustrated in the schematic in Figure 1D. The length of the colored bar represents the amount of analyte ions as indicated by the "Analyte level", whereas the forwarded solution dispersed ink into the storage channel to represent the "Volume level" (See Figure 1D). Consequently, a sample containing a certain concentration of the analyte provides a constant ratio of the analyte level to the volume level, independent of the introduced volume. Therefore, precise introductions are unnecessary for this device when the calibration curve is constructed by plotting the ratio of the detection channel length to the storage channel length against the concentrations of the analyte solutions.

RESULTS AND DISCUSSION

Sample Volume Estimation. With the proposed PADs, the storage channel is used to estimate the sample volume that is introduced downstream from the detection channel. When the sample volume is larger than that required to occupy the entire detection channel, the distance to the front of the solvent in the storage channel should be correlated with the introduced sample volume. Therefore, 60, 80, 100, 120, or 140 μL volumes of water were introduced into the PADs to measure the length from the introduction zone to the top of the solvent in the storage channel (S value). The S values were measured and plotted against the introduced volume. The relationship provided good linearity, as expressed in eq 2 (R^2 = 0.9841),

$$S = (V - V_0)/L \quad (2)$$

In eq 2, S is the length from the introduction zone to the top of the solvent in the storage channel (mm), V is the introduced volume (μL), V_0 is the volume that occupies the detection channel (μL), and L is the volume needed to fill a 1 mm length of the storage channel (μL mm^{-1}). In this study, the following equation was obtained: $S = (V - 23.5)/0.639$. Thus, we confirmed that the introduced volume is estimated using eq 2 by measuring the S value. The linear relationship is shown in Figure S2 in the Supporting Information.

Iron Determination. For iron determination, the reaction solution was printed at different numbers on the detection channel from one to five times. Figure 2 shows the photographs of the devices printed with different numbers of the reaction reagent, and the relationship between the printed number of the reagent and the ratio of the length of the red bar in the detection channel (D) to that from the introduction zone to the front of the solvent in the storage channel (S) (D/S ratio). The results indicate that the color intensity of the product was intensified as the number of printings increased, as shown in Figure 2A where an increased printing number shows a clear red color that could be recognized by the naked eye. However, the ratio of the detection zone length to the storage zone length is smaller, as shown in Figure 2B, when the number of printings is increased. Those results indicate that the measurable range is controllable by changing the printing time, although an increased number of printings provides a clear boundary in the detection channel.

According to the principle of the distance-readout PADs, the length of the red bar depends on the amount of iron ions contained in the sample[20] while the sample solution continuously flows forward from the detection channel into the storage channel. Printed blue lines represent the volume of the sample introduced into the introduction zone. Therefore, when we use the ratio of the length of the red bar in the

https://doi.org/10.1021/acsomega.2c08138
ACS Omega 2023, 8, 11213−11219

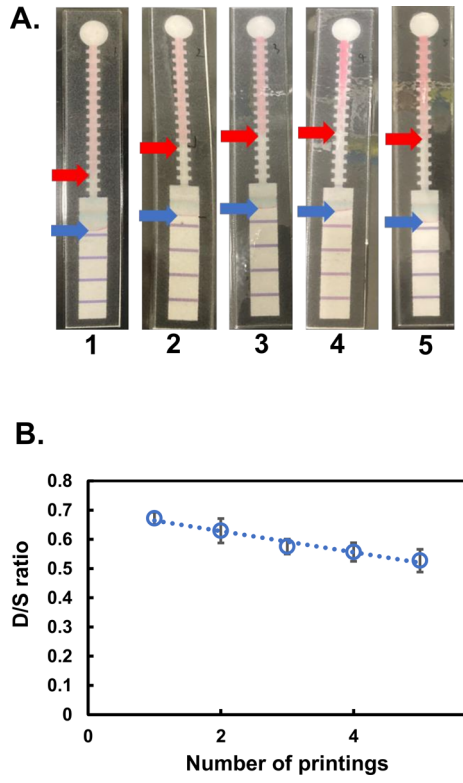

Figure 2. Effect of printing time; (A) images of the results for different printing times; and, (B) relationship between D/S ratios and the number of prints. The error bars indicate the standard deviations (n = 3).

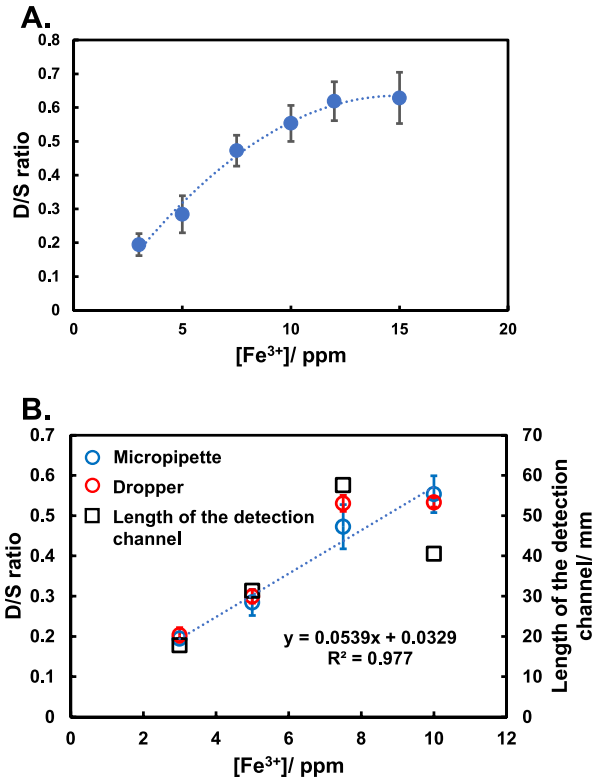

Figure 3. Iron determination; (A) relationship of the average D/S ratio to the concentration of iron; (B) calibration curves for iron determination using a micropipette or a dropper; (A) samples were introduced at volumes of 80, 100, 110, and 120 μL. The D/S ratios obtained by different volumes were averaged for each concentration; (B) blue circles, data obtained using a micropipette (the introduced volumes were 80, 100, 110, and 120 μL); and red circles were obtained using a dropper. The error bars indicate standard deviations.

detection channel (D) to that from the introduction zone to the front of the solvent in the storage channel (S) as an index to estimate the amounts of iron ions, precise introductions of samples are unnecessary.

To demonstrate a measurement that is independent of the introduced volume, the D/S ratios were plotted against the concentrations of iron ions by introducing different volumes (80, 100, 110, or 120 μL). When a sample contained a certain concentration of iron ions, the D/S ratio showed a constant value that was independent of the introduced volume. Table 1 shows the D/S ratios obtained by introducing different volumes of the samples at different concentrations. Table 1 shows that the D/S ratios were reproducible even when different sample volumes were introduced into the PADs in the range of 80−120 μL.

The calibration curves of iron ions with the PADs appear in Figure 3. The D/S ratios were saturated at a concentration range higher than 10 ppm (Figure 3A). The error bars in the calibration curve indicate the standard deviations of the D/S ratios obtained by introducing different volumes of samples (n = 3 for each introduction volume). Therefore, the D/S ratios provide appropriate signals that are independent of the introduced sample volumes.

The D/S ratio at 15 ppm is saturated because the entire detection zone is occupied by the red-colored complex. Therefore, the maximum measurable concentration is lower than 10 ppm under the present conditions. Conversely, when the iron concentration was below 3 ppm, the product showed a pale color that disrupted the color boundary. Therefore, the detection limit of the PAD was determined to be 3 ppm. The calibration curve provided a linearity range of 0 to 10 ppm with a good linear coefficient of 0.977 (Figure 3B). The black squares in Figure 3B indicate the colored length with no correction of the volume. It is apparent that the data of the absolute lengths at 7.5 and 10 ppm significantly deviate from a linear relationship. This would be because only a small

Table 1. D/S Ratios Obtained by the Introduction of Different Sample Volumes

	D/S ratio (average ± SD[a], n = 3)				
concentration of iron/ppm	80 μL	100 μL	110 μL	120 μL	average ± SD[b]
5	0.241 ± 0.034	0.330 ± 0.06	0.258 ± 0.025	0.309 ± 0.03	0.284 ± 0.054
7.5	0.496 ± 0.059	0.453 ± 0.018	0.504 ± 0.014	0.437 ± 0.035	0.473 ± 0.045
10	0.547 ± 0.045	0.536 ± 0.061	0.532 ± 0.043	0.599 ± 0.030	0.553 ± 0.053
15	0.538 ± 0.090	0.636 ± 0.025	0.678 ± 0.030	0.664 ± 0.038	0.629 ± 0.076

[a]SD, standard deviation. [b]The average and SD values were calculated from all data for individual concentrations (n = 12).

https://doi.org/10.1021/acsomega.2c08138
ACS Omega 2023, 8, 11213−11219

difference in introduced volume leads to a large difference in the absolute amount at high concentrations. The most important advantage of the present PAD is the ability to calibrate an analyte without precise sample introduction. The sample was then introduced onto the PAD using a plastic dropper. The data for the dropper are comparable to those of a micropipette, as shown in Figure 3B.

Effect of Viscosity. The viscosity of a sample may influence the flow rate in the channel of the PAD, and then, different D/S ratios will be obtained for samples with the same concentration of the analyte but with different viscosities. Therefore, we varied the viscosities of the sample with a constant concentration of iron by adding different concentrations of D (+)-glucose into the sample, i.e., the sample solutions contained 12 ppm of iron and 0, 0.25, 0.5, 0.75, or 1.0 M of D (+)-glucose.[33] The results show that the D/S ratio increases with an increase in sample viscosity, which is attributed to the decrease in the length of the storage channel for highly viscous samples (Figure S3, Supporting Information). In fact, the flow rate of the sample solution was decreased with an increase in the viscosity, resulting in a large D/S ratio probably due to the evaporation of the solution in the introduction zone. Therefore, the PADs must correct the effect of viscosity if the viscosity of the standard solution is significantly different from that of the sample solution.

BSA Determination. To confirm the applicability of the proposed PAD to viscous samples, the PADs were prepared for the determination of BSA in a serum sample. We noticed that the standard solutions with different concentrations of BSA had different viscosities when the solutions generated different degrees of bubbles after shaking. When the standard solutions were dropped onto a sample introduction zone via a dropper, they flowed into the detection channel, resulting in a color change from yellow to blue due to the ion-pair formation between BSA and TBPB. After dropping a sample, the PAD was left for 2 h and 30 min to dry completely.

The design of the PAD was modified for BSA determination because the blue color of the product in the detection channel was inhomogeneous when the detection channel was as wide as that for iron determination. The results of the determinations using PADs with different sizes of detection channels are shown in Figure 4. The channel size was reduced to 1, 2, or 3 mm. Although a large channel transported a solution rapidly, the blue bar was inhomogeneous for wider channels, as Figure 4 shows. The detection channel with a width of 1 mm showed a clearer boundary between yellow and blue than those with widths of 2 and 3 mm.

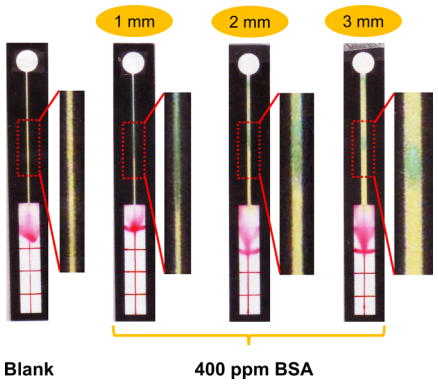

Figure 4. Effect of the channel size on the BSA determination. The width of the detection channel was varied at 1, 2, and 3 mm. One drop of a solution with 400 ppm BSA was added to the introduction zone using a dropper.

A calibration curve for BSA was constructed using the PADs with a 1 mm detection channel and a plastic dropper. A linear relationship was obtained between the average values of the D/S ratios and the concentration of BSA (D/S = 0.0015 (BSA concentration, ppm) + 0.0223, correlation coefficient; R^2 = 0.994, linear range; 0 to 400 ppm) (Figure S3, Supporting Information). The repeatability of the method in terms of the relative standard deviation (%RSD) was 5.16% for 200 ppm of BSA (n = 10). Although the standard solutions had different viscosities because of the BSA content, the PADs showed a good linear relationship in the determination of BSA (Figure S4, Supporting Information). This implies that viscosity is roughly proportional to concentrations of less than 1% (w/v)[34] and that the increase in viscosity is derived from BSA for the standard solutions. As a consequence, the effect of viscosity on the concentration measurement was negligible.

The PAD was then applied to the determination of BSA in a bovine serum sample. The sample was diluted to 0.25% due to its high concentration and viscosity. The results of the PAD were validated by comparing them with those of UV−visible spectrophotometry, which is a standard method for BSA determination where the absorbance of the complex between BSA and TBPB is measured at 625 nm. The PAD functioned at a concentration of 81.9 ppm, whereas the concentration obtained by spectrophotometry was 82.5 ppm, which shows good agreement between both systems.

CONCLUSIONS

Despite the fact that PADs are inherently simple, inexpensive, and easy to fabricate, users continue to need a micropipette to introduce a precise volume of a sample. The obvious necessity of the micropipette prevents its use by nonexperts in most cases. Therefore, we proposed a novel design for a PAD that could tolerate a rough volume of the sample and avoid the need of a micropipette for introducing samples. The proposed PADs simultaneously correct the sample volume and measure the analyte, according to simple distance-based readouts. The device permits the use of a plastic dropper instead of a micropipette since the storage channel of the PAD reports the volume of the sample introduced into the device. A proof-of-principle was successfully demonstrated in the determination of iron, and furthermore, the method was applied to the quantification of BSA. Calibration curves were constructed by plotting the D/S ratios, which are the ratios of the distance in the detection channel to that in the storage channel, against the concentration of the analyte. Regardless of the volume sizes, D/S ratios are constant for a sample containing a specific concentration of the analyte. Thus, the proposed PADs require no micropipette to quantify the target analyte and are more user-friendly and suitable for point-of-care testing outside of a laboratory.

ASSOCIATED CONTENT

Supporting Information

The Supporting Information is available free of charge at https://pubs.acs.org/doi/10.1021/acsomega.2c08138.

Relationship between the introduced volume and the length in the storage channel; relationship between

https://doi.org/10.1021/acsomega.2c08138
ACS Omega 2023, 8, 11213−11219

viscosity and the D/S ratio; and calibration curve for BSA (PDF)

AUTHOR INFORMATION

Corresponding Authors

Kaewta Danchana − *Department of Chemistry, Okayama University, Okayama 700-8530, Japan*; Email: kaewta@okayama-u.ac.jp

Takashi Kaneta − *Department of Chemistry, Okayama University, Okayama 700-8530, Japan*; orcid.org/0000-0001-9076-3906; Email: kaneta@okayama-u.ac.jp

Authors

Hiroshi Iwasaki − *Department of Chemistry, Okayama University, Okayama 700-8530, Japan*

Yada Thayawutthikun − *Flow Innovation-Research for Science and Technology Laboratories (FIRST Labs), Mahidol University, Bangkok 10400, Thailand; Department of Chemistry and Center of Excellence for Innovation in Chemistry, Faculty of Science, Mahidol University, Bangkok 10400, Thailand*

Phoonthawee Saetear − *Flow Innovation-Research for Science and Technology Laboratories (FIRST Labs), Mahidol University, Bangkok 10400, Thailand; Department of Chemistry and Center of Excellence for Innovation in Chemistry, Faculty of Science, Mahidol University, Bangkok 10400, Thailand*

Complete contact information is available at: https://pubs.acs.org/10.1021/acsomega.2c08138

Notes

The authors declare no competing financial interest.

ACKNOWLEDGMENTS

This research was supported by JSPS KAKENHI Grant number JP20H02766 and The Yakumo Foundation for Environmental Science.

REFERENCES

(1) Martinez, A. W.; Phillips, S. T.; Butte, M. J.; Whitesides, G. M. Patterned paper as a platform for inexpensive, low-volume, portable bioassays. *Angew. Chem., Int. Ed.* **2007**, *46*, 1318−1320.

(2) Yetisen, A. K.; Akram, M. S.; Lowe, C. R. Paper-based microfluidic point-of-care diagnostic devices. *Lab Chip* **2013**, *13*, 2210−2251.

(3) Wei, X.; Tian, T.; Jia, S.; Zhu, Z.; Ma, Y.; Sun, J.-J.; Lin, Z.; Yang, C. J. Microfluidic distance readout sweet hydrogel integrated paper-based analytical device (μdish-pad) for visual quantitative point-of-care testing. *Anal. Chem.* **2016**, *88*, 2345−2352.

(4) Karita, S.; Kaneta, T. Chelate titrations of Ca^{2+} and Mg^{2+} using microfluidic paper-based analytical devices. *Anal. Chim. Acta* **2016**, *924*, 60−67.

(5) Li, H.; Lin, H.; Wang, X.; Lv, W.; Li, F. Dopamine-based paper analytical device for truly equipment-free and naked-eye biosensing based on the target-initiated catalyzed oxidation. *ACS Appl. Mater. Interfaces* **2019**, *11*, 36469−36475.

(6) Taghizadeh-Behbahani, M.; Hemmateenejad, B.; Shamsipur, M.; Tavassoli, A. A paper-based length of stain analytical device for naked eye (readout-free) detection of cystic fibrosis. *Anal. Chim. Acta* **2019**, *1080*, 138−145.

(7) Ratnarathorn, N.; Dungchai, W. Paper-based Analytical Device (PAD) for the Determination of Borax, Salicylic Acid, Nitrite, and Nitrate by Colorimetric Methods. *J. Anal. Chem.* **2020**, *75*, 487−494.

(8) Seetasang, S.; Kaneta, T. Dip-and-read, organic solvent-compatible, paper-based analytical devices equipped with chromatographic separation for indole analysis in shrimp. *ACS Sens.* **2022**, *7*, 1194−1200.

(9) Renault, C.; Anderson, M. J.; Crooks, R. M. Electrochemistry in hollow-channel paper analytical devices. *J. Am. Chem. Soc.* **2014**, *136*, 4616−4623.

(10) Burkitt, R.; Sharp, D. Submicromolar quantification of pyocyanin in complex biological fluids using pad-printed carbon electrodes. *Electrochem. Commun.* **2017**, *78*, 43−46.

(11) Ding, R.; Cheong, Y. H.; Ahamed, A.; Lisak, G. Heavy metals detection with paper-based electrochemical sensors. *Anal. Chem.* **2021**, *93*, 1880−1888.

(12) Yamada, K.; Takaki, S.; Komuro, N.; Suzuki, K.; Citterio, D. An antibody-free microfluidic paper-based analytical device for the determination of tear fluid lactoferrin by fluorescence sensitization of Tb^{3+}. *Analyst* **2014**, *139*, 1637−1643.

(13) Qi, J.; Li, B.; Wang, X.; Fu, L.; Luo, L.; Chen, L. Rotational paper-based microfluidic-chip device for multiplexed and simultaneous fluorescence detection of phenolic pollutants based on a molecular-imprinting technique. *Anal. Chem.* **2018**, *90*, 11827−11834.

(14) Ireta-Muñoz, L. A.; Morales-Narváez, E. Smartphone and paper-based fluorescence reader: a do it yourself approach. *Biosensors* **2020**, *10*, 60.

(15) Liu, W.; Cassano, C. L.; Xu, X.; Fan, Z. H. Laminated paper-based analytical devices (LPAD) with origami-enabled chemiluminescence immunoassay for cotinine detection in mouse serum. *Anal. Chem.* **2013**, *85*, 10270−10276.

(16) Alahmad, W.; Uraisin, K.; Nacapricha, D.; Kaneta, T. A miniaturized chemiluminescence detection system for a microfluidic paper-based analytical device and its application to the determination of chromium (III). *Anal. Methods* **2016**, *8*, 5414−5420.

(17) Han, X.; Cao, M.; Wu, M.; Wang, Y.-J.; Yu, C.; Zhang, C.; Yu, H.; Wei, J.-F.; Li, L.; Huang, W. A paper-based chemiluminescence immunoassay device for rapid and high-throughput detection of allergen-specific IgE. *Analyst* **2019**, *144*, 2584−2593.

(18) Danchana, K.; Phansi, P.; de Souza, C. T.; Ferreira, S. L. C.; Cerdà, V. Spectrophotometric system based on a device created by 3D printing for the accommodation of a webcam chamber as a detection system. *Talanta* **2020**, *206*, No. 120250.

(19) Abramoff, M. D.; Magalhaes, P. J.; Ram, S. J. Image Processing with ImageJ. *Biophotonics Int.* **2004**, *11*, 36−42.

(20) Danchana, K.; Iwasaki, H.; Ochiai, K.; Namba, H.; Kaneta, T. Determination of glutamate using paper-based microfluidic devices with colorimetric detection for food samples. *Microchem. J.* **2022**, *179*, No. 107513.

(21) Channon, R. B.; Nguyen, M. P.; Henry, C. S.; Dandy, D. S. Multilayered Microfluidic Paper-Based Devices: Characterization, Modeling, and Perspectives. *Anal. Chem.* **2019**, *91*, 8966−8972.

(22) Alahmad, W.; Tungkijanansin, N.; Kaneta, T.; Varanusupakul, P. A colorimetric paper-based analytical device coupled with hollow fiber membrane liquid phase microextraction (HF-LPME) for highly sensitive detection of hexavalent chromium in water samples. *Talanta* **2018**, *190*, 78−84.

(23) Hopkins, H.; Oyibo, W.; Luchavez, J.; Mationg, M. L.; Asiimwe, C.; Albertini, A.; González, I. J.; Gatton, M. L.; Bell, D. Blood transfer devices for malaria rapid diagnostic tests: evaluation of accuracy, safety and ease of use. *Malar. J.* **2011**, *10*, 30.

(24) Yamada, K.; Citterio, D.; Henry, C. S. "Dip-and-read" paper-based analytical devices using distance-based detection with color screening. *Lab Chip* **2018**, *18*, 1485−1493.

(25) Komatsu, T.; Maeda, R.; Maeki, M.; Ishida, A.; Tani, H.; Tokeshi, M. Dip-type paper-based analytical device for straightforward quantitative detection without precise sample introduction. *ACS Sens.* **2021**, *6*, 1094−1102.

(26) Shimada, Y.; Kaneta, T. Highly sensitive paper-based analytical devices with the introduction of a large-volume sample via continuous flow. *Anal. Sci.* **2018**, *34*, 65−70.

(27) Hiraoka, R.; Kuwahara, K.; Wen, Y.-C.; Yen, T.-H.; Hiruta, Y.; Cheng, C.-M.; Citterio, D. Paper-based device for naked eye urinary albumin/creatinine ratio evaluation. *ACS Sens.* **2020**, *5*, 1110−1118.

(28) Channon, R. B.; Nguyen, M. P.; Scorzelli, A. G.; Henry, E. M.; Volckens, J.; Dandy, D. S.; Henry, C. S. Rapid flow in multilayer microfluidic paper-based analytical devices. *Lab Chip* **2018**, *18*, 793−802.
(29) Renault, C.; Li, X.; Fosdick, S. E.; Crooks, R. M. Hollow-channel paper analytical devices. *Anal. Chem.* **2013**, *85*, 7976−7979.
(30) Giokas, D. L.; Tsogas, G. Z.; Vlessidis, A. G. Programming fluid transport in paper-based microfluidic devices using razor-crafted open channels. *Anal. Chem.* **2014**, *86*, 6202−6207.
(31) Camplisson, C. K.; Schilling, K. M.; Pedrotti, W. L.; Stoneb, H. A.; Martinez, A. W. Two-ply channels for faster wicking in paper-based microfluidic devices. *Lab Chip* **2015**, *15*, 4461−4466.
(32) Adkins, J. A.; Noviana, E.; Henry, C. S. Development of a quasi-steady flow electrochemical paper-based analytical device. *Anal. Chem.* **2016**, *88*, 10639−10647.
(33) Vázquez, G.; Alvarez, E.; Navaza, J. Density, viscosity, and surface tension of sodium carbonate + sodium bicarbonate buffer solutions in the presence of glycerin, glucose, and sucrose from 25 to 40 °C. *J. Chem. Eng. Data* **1998**, *43*, 128−132.
(34) Yadav, S.; Shire, S. J.; Kalonia, D. S. Viscosity analysis of high concentration bovine serum albumin aqueous solutions. *Pharm. Res.* **2011**, *28*, 1973−1983.

https://doi.org/10.1021/acsomega.2c08138
ACS Omega 2023, 8, 11213−11219